IEEE Journal of Microwaves

Received 3 February 2021; revised 2 March 2021; accepted 2 March 2021. Date of current version 7 April 2021.

Digital Object Identifier 10.1109/JMW.2021.3065018

Complex Permittivity and Permeability Extraction of Ferromagnetic Materials For Magnetically Tuned Microwave Circuits

KHALED ALI ALHASSOON [1,2] (Member, IEEE), YAAQOUB MALALLAH [3] (Member, IEEE), AND AFSHIN S. DARYOUSH [1] (Fellow, IEEE)

(Invited Paper)

[1] Department of Electrical and Computer Engineering, Drexel University, Philadelphia, PA 19104 USA
[2] Department of Electrical Engineering, College of Engineering, Qassim University, Unaizah 737102, Saudi Arabia
[3] Energy and Building Research Center, Kuwait Institute for Scientific Research, Shuwaikh Educational, Kuwait City 70030, Kuwait

CORRESPONDING AUTHOR: AFSHIN S. DARYOUSH (e-mail: daryousa@drexel.edu).

This work is partially supported by Qassim University, Unaizah, Saudi Arabia.

ABSTRACT Ferromagnetic materials, such as ferrites, are employed for magnetically tuned radio frequency (RF) circuits. Ferrites exhibit both electric permittivity and magnetic permeability and independent RF characterization of these two properties is crucial for accurate design and modeling of RF circuits. A method that independently extracts each property over Wi-Fi frequencies is presented here, where complex permittivity and permeability of ferrite nano-particles are extracted using resonance frequency sensitivity of a 3D printed metallic cavity to various samples under test and their placement in the cavity. Air-filled 3D printed rectangular cavity using acrylonitrile butadiene styrene (ABS) are shielded using copper sheets; the structure of air-filled cavity is designed to excite TE_{101z} as the dominant resonance mode that resonates at 2.4 GHz. A cylindrical shape material under test (MUT) was added to the cavity at different positions for high electric and magnetic fields, while the resonant frequency change and degradation in quality factor of the resonant cavity are employed for accurate independent extraction of electric permittivity and magnetic permeability of MUT. The sample was prepared with volumetric distribution of 60:40 nanoparticles to glue ratio. In particular, a 3D printed composite sample of ABS with $NiFe_2O_4$ magnetic nanoparticles is placed in positions of high electric or high magnetic energy densities of the metallic cavity, while any changes in resonant frequency and its frequency selectivity are observed from the cavity insertion loss characteristics. Both perturbation theory (as analytical) and finite element method (as numerical) techniques are employed for extraction of complex permittivity and permeability of $NiFe_2O_4$. The perturbation theory provides accurate extraction, which is also numerically confirmed using curve fitting of the full wave simulated scattering parameters to the measured results.

INDEX TERMS Magnetic nanoparticles, NiFe2O4, magnetic permeability, electric permittivity, 3D printing, ABS, resonant cavity, perturbation theory, numerical extraction, finite-element method (FEM), resonant frequency, quality factor.

I. INTRODUCTION

Tunable radio frequency (RF) circuits are of great interest for advanced telecommunication systems. Tuning the resonance frequency of RF components extends the operating frequency range and enhances information security using frequency hopping techniques. In order to mitigate loading parasitic effects of frequency control circuits, it is prudent to employ ferromagnetic materials as tunable elements since it could be tuned by an externally applied magnetic field. Utilization of such materials is shown as self-biased by applying different thickness of NiCo ferrite film on patch antenna [1]–[2]. Another paper uses FeCo for antenna tuning after performing extraction using annular ring resonator [3]–[4]. The most important and common step among all reported papers

dealing with ferromagnetic materials is the characterization of the material at high frequency before proceeding with the design of RF circuits for different applications [5]–[6]. There are various materials that have been studied and used for RF applications such as $Fe_{60}Co_{40}$, $NiFe_2O_4$, and NiZnFeO magnetic nanoparticles as reported in the literature [7]–[8]. These physical characteristics of these materials vary based on the compound material, nanoparticle size, and the prepared ferromagnetic samples's structures.

Several approaches have been recently employed for characterization of all physical properties at radio frequencies: specifically, the extraction of ferromagnetic materials at high frequencies. The LCR Meter, Impedance Analyzer, and Nicholson-Ross-Weir (NRW) waveguide methods are well-known techniques that have been utilized to characterize materials at low frequency bands of under 1 GHz [9]. Malallah *et al.* reported microstrip transmission line and annular ring resonator to characterize ferromagnetic properties of $Fe_{60}Co_{40}$ nanoparticles material, since their permittivity is negligible [3]. The extraction of complex permeability of $Fe_{60}Co_{40}$ magnetic nanoparticles was achieved using best fitting of simulated to measured scattering (S)-parameters results of an enclosed annular ring resonator, while others employed TEM transmission line, such as coaxial discontinuity, test fixture, strip line [10]–[14] for extraction of permeabilities. Each method has a percentage error associated with the extraction procedure; for example, NRW method has reported an error of 5.8% over 1–10 GHz [9]. The TEM line extraction techniques are not convenient for accurate characterization of permittivity and permeability since electric and magnetic parameters and their contributions to electromagnetic energies are indistinguishable in TEM line printed circuit topologies. The proposed characterization method in this paper is based on rectangular metallic resonant cavity, where either electric or magnetic energies dominates at different positions. The placement of the ferrite sample accordingly could be employed to independently quantify electric permittivity or magnetic permeabilities.

Circular or rectangular [15]–[16] cavity structures have been utilized to characterize materials. The rectangular cavity resonator from a standard X-band waveguide was utilized to perform the measurement with and without the sample to extract the complex permeability of Nickel-Zinc ferrite-epoxy composite by perturbation technique [16]. The modified waveguide cavity was manufactured to have a slot on the top side to insert a rectangular shape sample. The measurement was performed on the sample that was placed in the middle of the cavity at odd and even modes [16]–[23]. This method of measurement and extraction was also reported by Zhu [11] where a slab was used instead of a rectangular sample. However, the same approach but with a cylindrical sample and a small radius in comparison to the cavity size is believed to have more accurate results. Another reported result show that performing the measurements at the same mode but at different sample positions based on the field strength of mode TE_{104} could be implemented [24]. It was found that the

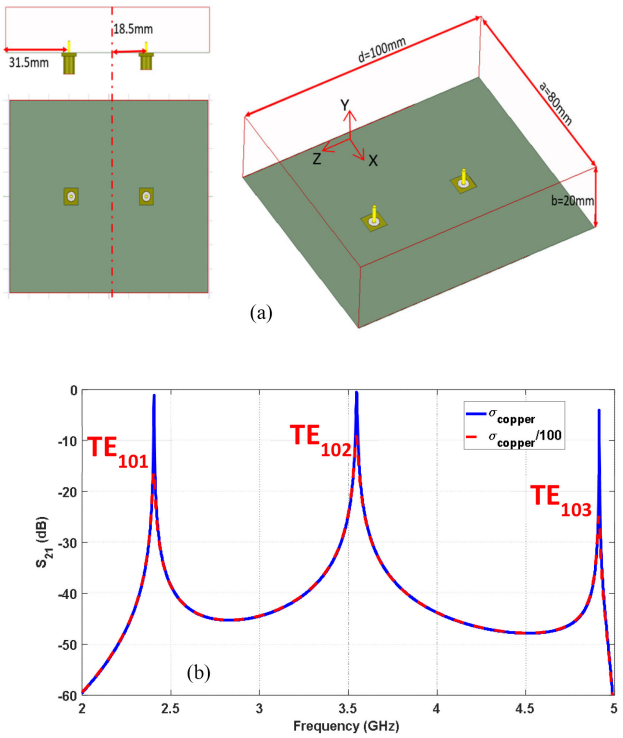

FIGURE 1. The air filled rectangular metallic cavity resonates at 2.4 GHz for dominant TE_{101z} mode. a) Cavity dimensions and model; b) comparison of insertion loss of the first three modes using a bulk copper (σ_{copper}) as material covering cavity versus a copper sheet metal with the fitted conductivity (σ_{copper}/100).

least square fit technique is the most reliable characterization procedure [25]. An improved rectangular cavity approach was reported by Jha [26], where the sample was placed horizontally to have higher field interaction. In this paper, a characterization procedure by using perturbation theory and curve fitting is reported. This is based on the measurement performed with 3D printed metallic cavity before and after introducing the ferromagnetic material under test (MUT).

II. DESIGN AND MODELING OF 3D PRINTED CAVITY

The design of air-filled metallic cavity was performed at 2.4 GHz, where dominant mode of TE_{101} is excited as TE_z. The dimensions of the cavity were calculated initially based on [26]:

$$f_0 = \frac{1}{2\pi\sqrt{\mu\varepsilon}}\left[\left(\frac{m\pi}{a}\right)^2 + \left(\frac{n\pi}{b}\right)^2 + \left(\frac{p\pi}{d}\right)^2\right]^2 \qquad (1)$$

where a, b, and d are the dimensions of the cavity as shown in Figure 1a; while m, n, and p are integer numbers designating the number of half cycles of the standing waves in x, y, and z directions. Two SMA connector soldered along the z axis to excite transverse plane electric fields required for TE_z in the metallic cavity. For this specific excitation there is limited information in the literature in regard to the optimum method of excitation. To maximize the coupled power to the cavity, the excitation is supposed to be strategically located for the optimum excitation of TE_{10z} traveling mode; the first three

TABLE 1. Calculation Of The Dominant Mode Of Electric And Magnetic Energy Densities For 1W Power Excitation

Parameters	Analytical	Numerical
$Eo = 2jE_{0y}^{+}$	$2277\frac{V}{m}$	$2722\frac{V}{m}$
$H_{0x}^{+} = -E_{0y}^{+}/Z_{TE_{10}} = Ho/2$	-5.60 A/m	-5.57 A/m
$Z_{TE_{10}} = \omega\mu/\beta$	482Ω	481.7Ω
$w_e(\mu W/cm^3) = \frac{\omega\epsilon'}{2}\left\|\boldsymbol{E}_{0\ p1}\right\|^2$	1.97	1.97
$w_m(\mu W/cm^3) = \frac{\omega\mu'}{2}\left\|\boldsymbol{H}_{0\ p1}\right\|^2$	0	$8.59\text{x}10^{-7}$
$w_e\ (\mu W/cm^3) = \frac{\omega\epsilon'}{2}\left\|\boldsymbol{E}_{0\ p2}\right\|^2$	$7.38\text{x}10^{-2}$	$7.54\text{x}10^{-2}$
$w_m(\mu W/cm^3) = \frac{\omega\mu'}{2}\left\|\boldsymbol{H}_{0\ p2}\right\|^2$	$3.31\text{x}10^{-1}$	$3.01\text{x}10^{-1}$

modes are shown in Figure 1b, when b<a<d. The unperturbed electromagnetic fields expression for the dominant TE_{101z} for the air-filled cavity is expressed as:

$$E_{0y} = E_0 \sin\left(\frac{\pi x}{a}\right)\sin\left(\frac{\pi z}{d}\right) \tag{2}$$

$$H_{0x} = H_0 \sin\left(\frac{\pi x}{a}\right)\cos\left(\frac{\pi z}{d}\right)$$

$$H_{0Z} = H_0 \cos\left(\frac{\pi x}{a}\right)\sin\left(\frac{\pi z}{d}\right) \tag{3}$$

It is important to note that the insertion loss reduces with lossy conductive materials. For example, Figure 1b depicts this phenomenon after considering the ohmic losses due to the lower conductivity of the oxidized copper sheet used to shield the 3D ABS printed cavity [27]. This is a crucial step as it will affect the curve fitting procedure later by reducing the achieved quality factor. The estimated conductivity of the copper sheet enclosure is lower by two orders of magnitude compared to the non-oxidized copper conductivity of $5.8\text{x}10^5$ S/cm; hence, the skin depth increases to be 13μm which is ten times higher than the non-oxidized copper skin depth. As a result, extra loss is introduced due to leakage of electromagnetic fields to the ABS enclosure. The comparison between the numerical and analytical approach in term of electric and magnetic field and related energy densities are listed in Table 1, where analytical expressions 2 and 3 are used for these calculations. Our numerical modeling of the perturbed cavity with ferrite samples is based on the full wave modeling using finite element method (FEM) simulations; particularly our FEM modeling of cavity structures are based on the Ansoft's high frequency structure simulator (HFSS).

Term Z_{TE} is defined in terms of resonant frequency of cavity and is expressed in unit of Ω as $377/\sqrt{1-f_c/f_0}$. It can be seen clearly that simulation and the analytical calculations are matched for the air-filled cavity, which is the baseline for our measurement [28]. The dominant excited mode was TE_{101z} which was used for extraction since it is suitable for perturbational method because the maximums of electric and magnetic fields are at 2 different locations in the cavity. Therefore, based on the measurement type that is going

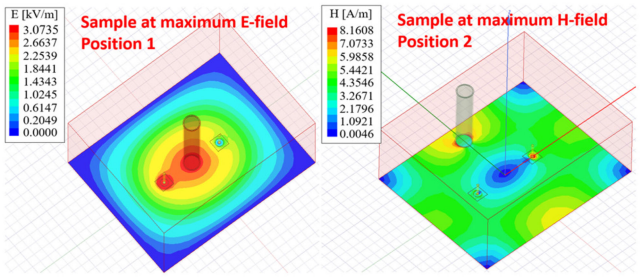

FIGURE 2. The simulated strength of perturbed electromagnetic fields for resonant cavity with cylindrical 3D printed ABS sample of r=4mm, h=5mm placed for 1 W excitation; a) MUT placed at peak electric field of P_1. Red is peak of 3kV/m and dark blue is 0 V/m in steps of 0.4kV/m.; b) MUT placed close to wall at position P_2. Red is peak of 8A/m and dark blue is 0 A/m in steps of 1 A/m.

to be performed, the sample could be inserted at maximum electric field intensity (P_1: center) or magnetic field intensity (P_2: close to walls), as shown for fields in Figure 2.

This characterization technique has the advantage of extracting complex permittivity and permeability individually using perturbation theory, as long as sample volume is significantly smaller than cavity volume. However, the volume of the sample must be small with respect to the cavity which means it has to be less than one tenth the volume of the cavity. The perturbation theory is based on approximating the revised field intensity due to placement of sample remains very similar to the empty cavity case. By measuring the change in the resonance frequency and quality factor, when the MUT is placed at either maximum electric or magnetic fields [29] for the dominant mode, then the complex permeability and permittivity could be quantified. This change in resonance frequency due to a sample is represented [29]

$$\frac{\omega-\omega_0}{\omega_0} = -\frac{\iiint_{V_S}\left(\Delta\varepsilon\boldsymbol{E}.\boldsymbol{E}_0^* + \Delta\mu\boldsymbol{H}.\boldsymbol{H}_0^*\right)dV}{\iiint_{V_0}\left(\varepsilon_0\boldsymbol{E}.\boldsymbol{E}_0^* + \mu_0\boldsymbol{H}.\boldsymbol{H}_0^*\right)dV} \tag{4}$$

where $\boldsymbol{E}_0$ *and* $\boldsymbol{H}_0$ represent the un-perturbed electric and magnetic fields, and ω_0 resonance frequency of the air-filled cavity; while $\boldsymbol{E}$, $\boldsymbol{H}$ *and* ω correspond to the perturbed case. $\Delta\varepsilon$ and $\Delta\mu$ are the change in the permittivity and permeability after introducing the MUT. V_0 and V_s are the volumes of the full cavity and sample, respectively. This is the starting step to quantify the complex permittivity and permeability. Perturbation technique is based on the assumption that the fields remain almost the same after introducing the small sample. Moreover, once the sample is placed at either maximum electric or maximum magnetic field intensities, the corresponding magnetic or electric energy densities are very small and can be ignored.

Based on the resonance principle, an equi-partition of the electric and magnetic energy densities correspond to $W_e = W_m$:

$$\varepsilon_0\iiint_{V_0}\left(|\boldsymbol{E}_0|^2\right)dV = \mu_0\iiint_{V_0}\left(|\boldsymbol{H}_0|^2\right)dV \tag{5}$$

Thus, using equipartition of energy and recognizing sample is placed at high electric energy density and zero magnetic energy (i.e., position P_1), then (4) is approximated:

$$\frac{\omega-\omega_0}{\omega o} \approx -\frac{\iiint_{V_S} \Delta\varepsilon \left(\boldsymbol{E}_0.\boldsymbol{E}_0^*\right) dV}{2\varepsilon_0 \iiint_{V_0} \left(|\boldsymbol{E}_0|^2\right) dV} \tag{6}$$

Meanwhile, the difference in permittivity is represented by $\Delta\varepsilon = \varepsilon - \varepsilon_0$ with $\varepsilon = \varepsilon_r\varepsilon_0$, while the complex relative permittivity is $\varepsilon_r = \varepsilon_r' - j\varepsilon_r''$. Therefore, (6) is approximated to even a simpler expression for a sample placed in the position P_1 of a maximum electric energy, while magnetic energy is minimized:

$$\frac{\omega-\omega_0}{\omega_o} \approx -\frac{(\varepsilon_r-1)\iiint_{V_S} \left(\boldsymbol{E}_0.\boldsymbol{E}_0^*\right) dV}{2\iiint_{V_0} \left(|\boldsymbol{E}_0|^2\right) dV} \tag{7}$$

Adding the sample into the air-filled cavity introduces additional losses to the system. In fact, a complex angular frequency represented as $\omega = \omega_r - j\omega_j$, which relates real part of electric permittivity to change in resonant frequency and imaginary part of electric permittivity to the cavity quality factor as $Q \approx \omega_r/2\omega_j$, then the following relationship exists:

$$\frac{\delta\omega}{\omega} = \frac{\omega_s-\omega_0}{\omega_s} = \frac{f_s-f_0}{f_s} + \frac{j}{2}\left(\frac{1}{Q_s} - \frac{1}{Q_0}\right) \tag{8}$$

where $\omega = 2\pi f, Q_0 \approx f_0/\Delta f$ is the quality factor of air-filled cavity, and $Q_s \approx f_s/\Delta f$ the quality factor of the perturbed cavity with subscript "s" signifying cavity with the sample. We can establish the link between theory of perturbation (7) and bandwidth (8), as shown in (9):

$$-\frac{(\varepsilon_r-1)\iiint_{V_S} \left(|\boldsymbol{E}o|^2\right) dV}{2\iiint_{V_0} \left(|\boldsymbol{E}o|^2\right) dV} = \left(\frac{f_s-f_0}{f_s}\right) + \frac{j}{2}\left(\frac{1}{Q_s} - \frac{1}{Q_0}\right) \tag{9}$$

Thus, a filling coefficient of N is defined as:

$$N = \frac{\iiint_{V_S} \left(|\boldsymbol{E}_0|^2\right) dV}{\iiint_{V_0} \left(|\boldsymbol{E}_0|^2\right) dV} = \frac{4\pi r^2}{ad} \tag{10}$$

which depends on the cavity and sample volumes. Since, the electric field of TE_{101} mode is in the y-axis direction and as indicated in (2), then this equation can be rewritten as:

$$-N_{p1}\,(\varepsilon_r-1) = 2\frac{f_s-f_0}{f_s} + j\left(\frac{1}{Q_{sp1}} - \frac{1}{Q_0}\right) \tag{11}$$

As a result of algebraic manipulations on (11), the calculated complex relative permittivity using perturbation theory is:

$$\varepsilon_r' = 1 + \frac{2}{N_{p1}}\frac{f_0-f_{sp1}}{f_{sp1}} \varepsilon_r'' = \frac{1}{N_{p1}}\left(\frac{1}{Q_{sp1}} - \frac{1}{Q_0}\right) \tag{12}$$

To extract the complex permeability, the same concept will be applied but by placing the sample at the position P_2, which is close to the cavity's side wall as shown Figure 2b. However, at this position electric field is non-zero. As a result, the change in (4) with respect to the magnetic field is related by:

$$\frac{\omega-\omega_0}{\omega o} \approx -\frac{\iiint_{V_S} \left(\Delta\varepsilon \boldsymbol{E}_0.\boldsymbol{E}_0^* + \Delta\mu \boldsymbol{H}_0.\boldsymbol{H}_0^*\right) dV}{2\iiint_{V_0} \left(\mu_0 \boldsymbol{H}_0.\boldsymbol{H}_0^*\right) dV} \tag{13}$$

The electric field impacts on the sample is small and does not alter the extracted results at position 2. Table 1 shows that the $W_e < W_m$ and electric energy contributions has limited effect on the change in resonance frequency or quality factor. Thus, the following equations assume $\mathbf{E}_0$ is very small and ignored for position P_2. Also, the filling factor based on (3) is:

$$N_{p2} = \frac{\pi r^2}{ad}\frac{2}{1+(d/a)^2} \tag{14}$$

Therefore, the calculated complex relative permeability is:

$$\mu_r' = 1 + \frac{1}{N}\frac{f_{0-}f_{sp2}}{f_{sp2}} \mu_r'' = \frac{1}{2N_{p2}}\left(\frac{1}{Q_{sp2}} - \frac{1}{Q_0}\right) \tag{15}$$

By applying the perturbation theory analysis, both permittivity and permeability of any material could be extracted at any desired resonance frequency. Moreover, by taking advantage of the flexible manufacturing of 3D printing, cavity fabrication is repeatable at wide range of frequencies. This procedure provides option to extract electric permittivity and magnetic permeability of ferrites. The second approach of extraction is based on curve fitting of simulated to measured insertion loss using full-wave numerical simulation using FEM (e.g., Ansoft's HFSS). This accurate extraction procedure is performed iteratively by starting from the approximate analytically calculated values until the least square error is achieved between the measured and simulated insertion loss of cavity with sample under test. The process of curve fitting was previously reported in detail [30]–[33] for extraction of various material properties, such as dielectric (RT/Duroid, PLA, ABS, …), magnetic nano-particles (FeCo), and metals (copper, MXene, …), but not to ferrites thus far.

III. 3D PRINTING OF CAVITY AND CHARACTERIZATION OF THE MAGNETIC NANOPARTICLES

The fabrication of metallic cavities using additive manufacturing provides an independent and flexible way to realize different geometrical shapes. Fabricating the metallic cavity is achieved by 3D printing the mold of the cavity first after modelling it with CAD software; then it is shielded with copper sheets. The required 3D printing time depends on the infill percentage of filament to air. For example, the printed cavity with 100% infill takes approximately 4-6 hours. However, this time can be adjusted by changing different settings of the 3D printer, such as their printing pattern.

The cavity with dimensions shown in Figure 1a was printed in 2 stages: i) the basic rectangular shape of cavity enclosure is printed first with appropriate holes for connecting SMA connectors as probe, ii) print 3 different shape lids. These lids are associated with 4 different cover cases of cavity: i) empty cavity cover as the baseline design, ii) a cover with cylindrical sample holder using ABS for position P_1 of cavity without

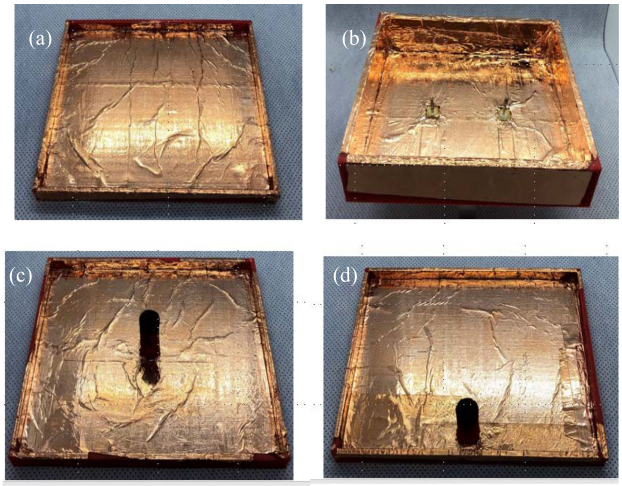

FIGURE 3 Fabrication process of 3D printed metallic cavity with dimensions of a= 8cm, b= 2cm, d= 10cm and perturbed by samples under test; a) lid with metallic enclosure; b) base with SMA probes ;c) lid for a sample placed at the center (position P_1); d) lid for sample placed at the edge of cavity (position P_2).

TABLE 2 Comparison Of Measured And Simulated Resonance Frequency And Quality Factor Of The Unperturbed Rectangular Metallic Cavity

Unperturbed Cavity	TE_{101z} Resonance (GHz)	S_{21} (dB)	$\Delta f = BW$ (MHz)	$Q \approx f/\Delta f$
Simulation	2.40	15	13	185
Measurement	2.40	15	13	185

ferromagnetic sample inside, iii) a cover of (ii) filled with ferromagnetic material also located at P_1 of cavity, iv) a cover with cylindrical sample holder filled with ferromagnetic material and placed at the edge of cavity in position P_2. This means with 4 different covers with the same base of the cavity will provide four separate measurements and the only difference is in the cover lid structure. This reduces the error associated with using different cavities and reconnecting cables.

Table 2 tabulates performance of the unperturbed cavity at 2.4 GHz with a narrow bandwidth, which implies a high quality factor. Figure 3 describes the fabrication process. The lid and base are printed with ABS filament. Then copper sheet tape is attached to the ABS lid of the cavity, as depicted in Figure 3a. Afterward, the SMA connectors are inserted and soldered to the base, as shown in Figure 3b. Finally, the lid with copper sheet tape attached on the inside encloses the cavity. Meanwhile, the other two lids were loaded with nanoparticles as shown in Figure 3c and Figure 3d. The nanoparticles of $NiFe_2O_4$ were mixed with Norland glue before loading it into the sample container on the lids. The mixture is volumetrically distributed with 60% nanoparticles and 40% Norland glue; Norland glue is solidified by UV light exposure. Various sizes of the cylindrical sample container were also studied to achieve optimum extractions results. The optimum volume has the same height as the unperturbed cavity with cylinder radius of 4 mm.

TABLE 3. Characteristics Of Perturbed Rectangular Metallic Cavity With ABS and Composite Nanoparticles Samples At The Positions P_1 (center) and P_2 (edge) of the Cavity. ^{M} = Measured, ^{S} = Simulated Using HFSS Curve Fitting Technique

MUT Type/ Position	ABS/ P_1	$NiFe_2O_4$/ P_1	$NiFe_2O_4$/ P_2
TE_{101} Resonance (GHz)	2.36^S 2.36^M	2.33^S 2.33^M	2.38^S 2.38^M
S_{21} (dB)	18^S 19^M	22^S 22^M	23^S 23^M
Δf =BW (MHz)	17^S 17^M	22^S 22^M	25^S 29^M
$Q \approx f/\Delta f$	145^S 145^M	105^S 105^M	80^S 80^M

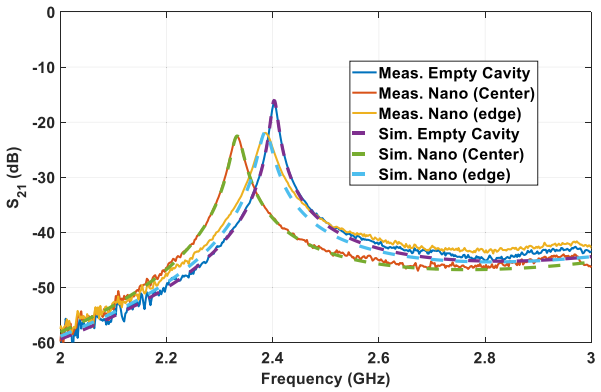

FIGURE 4. Measured and simulated S_{21} of the unperturbed and perturbed metallic cavity with ABS as MUT at the center of cavity.

IV. EXTRACTION OF COMPLEX PERMEABILITY & PERMITTIVITY OF THE MUT

The next characterization step is to perform the measurement of 3D printed ABS with and without composite nanoparticles at different positions of the empty cavity. Cavity cover lids of Figure 3c and Figure 3d are employed for $NiFe_2O_4$ sample positions of P_1 (high electric field) and P_2 (dominant magnetic field over electric field) in the cavity. Table 3 tabulates the amount of change in the resonance frequency and quality factor based on placing different MUT (ABS and ABS with ferromagnetic nanoparticles samples) at positions of P_1 and P_2 based on the $|S_{21}|$ measurement results, as depicted in Figure 4 and Figure 5.

The overall resonance frequencies behavior of the perturbed cavity after introducing the samples are shifted downward by different amounts. This is due to the change on the refractive index. Moreover, the bandwidth increases as we introduce samples due to the added dielectric loss. Comparison of the curve fitted insertion loss of ABS with measurement is depicted in Figure 4. Equations (12) and (15) are employed to extract the complex permittivity and permeability - listed in Table 3 – from resonance frequency tuning and changes in

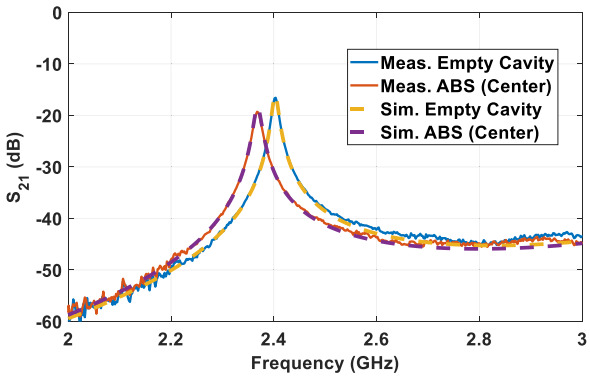

FIGURE 5. **Insertion loss of metallic cavity empty and partially filled with the 3D printed $NiFe_2O_4$ sample at positions P_1 (center) and P_2 (edge), where peaks of electric field and magnetic fields occurs respectively.**

TABLE 4. **Comparison of Extracted Properties of the MUT Samples at the Positions P_1 (Center) and P_2 (Edge) of the Cavity By Utilizing Perturbational Theory (^{A} = Analytical) and Curve Fitting (^{N} = Numerical) Techniques**

MUT Type and Position	ABS P_1	$NiFe_2O_4$ P_1	$NiFe_2O_4$ P_2
ε'_r	2.3^N 2.5^A	3.1^N 3.4^A	3.1^N 3.4^A
ε''_r	0.05^N 0.06^A	0.15^N 0.17^A	0.15^N 0.17^A
Tanδ	0.02^N 0.03^A	0.05^N 0.05^A	0.05^N 0.05^A
μ'_r	1^N 1^A	- -	2.5^N 2.5^A
μ''_r	0^N 0^A	- -	0.87^N 0.77^A
Tanδ	0^N 0^A	- -	0.35^N 0.30^A

quality factor. The real part of permittivity is higher than the real part of permeability which explains a higher downward shift in resonance frequency of P_1 versus P_2 positions for a similar sample size. However, the imaginary part of permeability is four times the imaginary part of permittivity, which implies a lossy magnetically tuned circuit.

The extracted results using perturbation technique are used as seed for more accurate full-wave numerical simulation of the cavity. The simulated results were curve fitted to the measured S-parameters using HFSS simulation as shown in Figure 5. The curve fitted results were performed with extracting the permittivity while the relative permeability was set to be 1-j0. This is because when the sample is at the center where the highest electric field is, the impact on the permeability due to the magnetic field is minimum or none. A similar process was applied for extracting the permeability. From Table 4, one can calculate the complex permittivity of 3D to be 2.5-j0.06 using perturbational theory (13). Meanwhile, the more accurate curve fitting extraction technique has a lower complex permittivity with by 8% difference in comparison with perturbation results. The calculated perturbational theory results match the curve fitting technique results with less than 10% error for all the extracted values.

V. CONCLUSION

Tunable RF circuits play an important part in the secure telecommunication systems such as frequency hopping and use of tunable frequency selective surfaces. The composite $NiFe_2O_4$ nanoparticles material was characterized at 2.4 GHz using measurements of cavity resonance frequency and quality factor. The perturbation theory provides the ability to characterize the complex permittivity and permeability independently by placement of sample in the regions of high electric and magnetic field regions. Independent extractions of complex permittivity and permeability can be used for RF characterization of various ferromagnetic material for design of magnetically tuned RF circuits [31].

Unfortunately, the lossy nature of the ferrite magnetic nanoparticles limits RF circuit performance, which could be only circumvented by material development of new magnetic nanoparticles or engineering solutions of artificial materials using electromagnetic bandgap engineering (EBG). The slow-wave group velocity characteristics of EBG pattern of $NiFe_2O_4$ is taken advantage of to enhance frequency tuning responsivity of the magnetically tuned annular ring resonators and antennas [34].

REFERENCES

[1] Z.-.B. Lin, J. J.-Q. Lin, and S. Robin, "A compact broadband tunable antenna with sophisticated performance," in *Proc. IEEE Antennas Propag. Soc. Int. Symp.*, 2008, pp. 1–4.

[2] G. Yang *et al.*, "Planar circular loop antennas with self-biased magnetic film loading," *Electron. Lett.*, vol. 44, no. 5, 2008.

[3] G. Yang *et al.*, "Electronically tunable miniaturized antennas on magnetoelectric," *IEEE Trans. Magn.*, vol. 44, no. 11, pp. 3091–3094, Nov. 2008.

[4] Y. Malallah, A. Singh, S. Deshmukh, C. Chinnasamy, M. Marinescu, and A. Daryoush, "Complex permeability extraction of feco nanoparticles using annular ring resonator and its RF applications," *J. Franklin Inst.*, 2017.

[5] K. Alhassoon, Y. Malallah, C. Chinnasamy, M. Marinescu, and A. Daryoush, "High gain tunable stacked antenna using soft FeCo nanoparticles," in *Proc. IEEE Radio Wireless Symp.*, 2016, pp. 1–4.

[6] M. V. Ghaffar, M. Farooqui, and A. Shamim, "A ferrite nano-particles based fully printed process for tunable microwave components," in *Proc. IEEE MTT-S Int. Microw. Symp.*, 2016, pp. 1–4.

[7] A. Shamim, J. R. Bray, N. Hojjat, and L. Roy, "Ferrite LTCC-Based antennas for tunable SoP applications," *IEEE Trans. Compon., Packag. Manuf. Technol.*, vol. 1, no. 7, pp. 999–1006, Jul. 2011.

[8] T. Okamura, T. Fujimura, and M. Date, "Dielectric constant and permeability of various ferrites in the microwave region," *Phys. Rev.*, vol. 85, no. 6, 1952, Art. no. 1041.

[9] H. Zhao, X. Sun, C. Mao, and J. Du, "Preparation and microwave–absorbing properties of nife2o4-polystyrene composites," *Physica B, Condens. Matter*, vol. 404, no. 1, pp. 69–72, 2009.

[10] P. I. Deffenbaugh, R. C. Rumpf, and K. H. Church, "Broadband microwave frequency characterization of 3-D printed materials," *IEEE Trans. Compon., Packag. Manuf. Technol.*, vol. 3, no. 12, pp. 2147–2155, Dec. 2013.

[11] S. C. Zhu, H. Y. Chen, and F. P. Wen, "Measurement theory and experimental research on microwave permeability and permittivity by using the cavity characteristic equation method," *IEEE Trans. Magn.*, vol. 28, no. 5, pp. 3213–3215, Sep. 1992.

[12] A. Verma, A. K. Saxena, and D. C. Dube, "Microwave permittivity and permeability of ferrite–polymer thick films," *J. Magn. Magn. Mater.*, vol. 263, no. 1-2, pp. 228–234, 2002.
[13] N. E. Belhadj-Tahar, A. Fourrier-Lamer, and H. De Chanterac, "Broadband simultaneous measurement of complex permittivity and permeability using a coaxial discontinuity," *IEEE Trans. Microw. Theory Techn.*, vol. 38, no. 1, pp. 1–7, Jan. 1990.
[14] C. Morales, "Tunable magneto-dielectric polymer nanocomposites for microwave applications," *IEEE Trans. Microw. Theory Techn.*, vol. 59, no. 2, pp. 302–310, Feb. 2011.
[15] W. Barry, "A broad-band, automated, stripline technique for the simultaneous measurement of complex permittivity and permeability," *IEEE Trans. Microw. Theory Techn.*, vol. 34, no. 1, pp. 80–84, Jan. 1986.
[16] T. Rydholm, "Measurement of complex permittivity and permeability through a cavity perturbation method," Ph.D. dissertation, MS Thesis, Chalmers University of Technology, Gothenburg, Sweeden, 2015.
[17] A. Verma, A. K. Saxena, and D. C. Dube, "Microwave permittivity and permeability of ferrite–polymer thick films," *J. Magn. Magn. Mater.*, vol. 263, no. 1-2, pp. 228–234, 2003.
[18] Y. Ye, A. Sklyuyev, C. Akyel, and P. Ciureanu, "Automatic system to measure complex permittivity and permeability using cavity perturbation techniques," in *Proc. IEEE Instrum. Meas. Technol. Conf. (IMTC)*, 2007, pp. 1–6.
[19] Z. Peng, J. Y. Hwang, and M. Andriese, "Maximum sample volume for permittivity measurements by cavity perturbation technique," *IEEE Trans. Instrum. Meas.*, vol. 63, no. 2, pp. 450–455, Feb. 2014.
[20] K. P. Thakur and W. S. Holmes, "An inverse technique to evaluate permittivity of material in a cavity," *IEEE Trans. Microw. Theory Techn.*, vol. 49, no. 6, pp. 1129–1132, Jun. 2001.
[21] L. Chen, C. K. Ong, and B. T. G. Tan, "Amendment of cavity perturbation method for permittivity measurement of extremely low-loss dielectrics," *IEEE Trans. Instrum. Meas.*, vol. 48, no. 6, pp. 1031–1037, Dec. 1999.
[22] J. Sheen, "Amendment of cavity perturbation technique for loss tangent measurement at microwave frequencies," *J. Appl. Phys.*, vol. 102, no. 1, 2007, Art. no. 014102.
[23] J. Sheen, C. Y. Li, and S. W. Lin, "Measurements of microwave dielectric properties of (1-x) TiO_2-x$CaTiO_3$ and (1-x) TiO_2-x$SrTiO_3$ thin films by the cavity perturbation method," *J. Electromagn. Waves Appl.*, vol. 25, no. 13, pp. 1886–1894, 2011.
[24] A. K. Jha and M. J. Akhtar, "A generalized rectangular cavity approach for determination of complex permittivity of materials," *IEEE Trans. Instrum. Meas.*, vol. 63, no. 11, pp. 2632–2641, Nov. 2014.
[25] A. Sklyuyev, M. Ciureanu, C. Akyel, P. Ciureanu, D. Menard, and A. Yelon, "Measurement of complex permeability of ferromagnetic nanowires using cavity perturbation techniques," in *Proc. IEEE Can. Conf. Elect. Comput. Eng.*, 2006, pp. 1486–1489.
[26] A. K. Jha and M. J. Akhtar, "An improved rectangular cavity approach for measurement of complex permeability of materials," *IEEE Trans. Instrum. Meas.*, vol. 64, no. 4, pp. 995–1003, Apr. 2015.
[27] M. N. Afsar, J. R. Birch, R. N. Clarke, and G. W. Chantry, "The measurement of the properties of materials," *Proc. IEEE*, vol. 74, no. 1, pp. 183–199, 1986.
[28] J.-H. Park and J.-G. Park, "Uncertainty analysis of Q-factor measurement in cavity resonator method by electromagnetic simulation," *SN Appl. Sci.*, vol. 2, no. 5 pp. 1–6, 2020.
[29] R. Harrington, *Time-Harmonic Electromagnetic Fields*. New York, NY, USA: McGraw-Hill, 1961, pp. 127–130.
[30] K. Alhassoon, Y. Malallah, J. J. Alcantar-Peña, N. Kumar, and A. S. Daryoush, "Broadband RF characterization and extraction of material properties in 3-D printed composite substrates for magnetically tuned circuits," *IEEE Trans. Microw. Theory Techn.*, vol. 69, no. 3, pp. 1703–1710, Mar. 2021.
[31] Y. Malallah, C. Chinnasamy, K. Alhassoon, and A. Daryoush, "Broadband permeability extraction of soft magnetically tunable Fe–Co nanoparticles," *IEEE Microw. Wireless Compon. Lett.*, vol. 29, no. 6, pp. 433–435, Jun. 2019.
[32] K. AlHassoon *et al.*, "Conductivity extraction of thin $Ti_3C_2T_x$ MXene films over 1–10 GHz using capacitively coupled test-fixture," *Appl. Phys. Lett.*, vol. 116, no. 18, 2020, Art. no. 184101.
[33] M. Hadjloum, M. E. Gibari, H. Li, and A. S. Daryoush, "An ultra-wideband dielectric material characterization method using grounded coplanar waveguide and genetic algorithm optimization," *Appl. Phys. Lett.*, vol. 107, no. 14, Oct. 2015, Art. no. 142908.
[34] K. AlHassoon, "Magnetically tuned 3D printed antenna arrays," Ph.D. dissertation, Dept. ECE, Drexel Univ., 2020.

KHALED ALHASSOON (Member, IEEE) received the B.S. degree from Qassim University, Saudi Arabia, in 2011, and the M.S. and Ph.D degrees, under the supervision of Dr. Afshin Daryoush, from Drexel University, Philadelphia, PA, USA, in 2016 and 2020, respectively. From 2012 to 2013, he was a Teacher Assistant with Qassim University, before receiving the scholarship for his graduation from Drexel University. Since August 2020, he has been a Faculty Member with Qassim University.

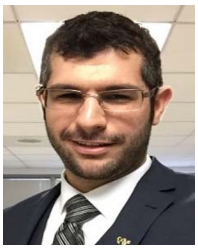

YAAQOUB MALALLAH (Member, IEEE) received the B.S.E.E degree *(summa cum laude)* from Temple University, Philadelphia, PA, USA, in 2010, and the M.S. degree and the Ph.D. degree, on the topic of ferroics and applications in tunable RF circuits, from Drexel University, Philadelphia, PA, USA, in 2012 and 2018, respectively. He is currently an Assistant Research Scientist with Kuwait Institute for Scientific Research. His current research interests include tunable microwave circuits employed in electromagnetics field and antenna systems, and energy harvesting and energy transmission, using wireless technologies.

AFSHIN S. DARYOUSH (Fellow, IEEE) received the B.S. degree in electrical engineering from Case Western Reserve University, Cleveland, OH, USA, in 1981, and the M.S. and Ph.D. degrees in electrical engineering from Drexel University, Philadelphia, PA, USA, in 1984 and 1986, respectively. He joined as a Dupont Assistant Professor with Drexel University, where he has developed more than 20 new courses and restructured six courses in devices, circuits, and systems for fundamentals of electrical and computer engineering. He has authored or coauthored more than 450 technical papers, ten book chapters, and 23 patents, where 16 have already been awarded. His research focuses on microwave photonics applied to telecommunications and biomedical engineering. He was the recipient of the Microwave Prize in 1986, and 15 papers have been recognized as the best student papers in various IEEE conferences. He received the Drexel University's Graduate Teaching Award in 2000, the IEEE Philadelphia Section's Franklin Key Award in 2015, the Drexel University's Alumni Award in 2018, and the Drexel's College of Engineering Innovation Award in 2020. From 1993 to 1995 and since 2014, he has been with the Institute of Electrical and Electronic Engineers (IEEE) in capacities of Chair of the Philadelphia joint AP/MTT Chapter, a Founding Faculty Advisor to the Drexel's IEEE Graduate Student Chapter since 2007, a Member of IEEE publications from 1998 to 2001, an IEEE Fellow Selection Committee in 2014, and since 2021, he has been the Chair of the MTT-22 Technical Committee. Since 1993, he has been organizing various IEEE conferences, and was the TPC Chair of RWS2008 and the General Chair of RWW2009, MWP2010, and BenMAS2014, and the Co-Chair of IMS2018, MWP2012, MWP2013, and MWP2019. Since 1986 and 2011, he has been a Member of the Sigma-Xi and Franklin Institute's Committee on Science and the Arts respectively.